SCIENTIFIC REPORTS

OPEN

SUBJECT AREAS:
PHYSICS
MATERIALS SCIENCE
NANOSCIENCE AND TECHNOLOGY

Received
12 October 2014

Accepted
24 December 2014

Published
27 January 2015

Correspondence and requests for materials should be addressed to U.S. (udo.schwingenschlogl@kaust.edu.sa)

Effect of Gd doping and O deficiency on the Curie temperature of EuO

Nuttachai Jutong[1], Ulrich Eckern[1], Thomas Mairoser[2] & Udo Schwingenschlögl[3]

[1]Institut für Physik, Universität Augsburg, 86135 Augsburg, Germany, [2]Zentrum für elektronische Korrelationen und Magnetismus, Universität Augsburg, 86159 Augsburg, Germany, [3]KAUST, PSE Division, Thuwal 23955-6900, Kingdom of Saudi Arabia.

The effect of Gd doping and O deficiency on the electronic structure, exchange interaction, and Curie temperature of EuO in the cubic and tetragonal phases is studied by means of density functional theory. For both defects, the Curie temperature is found to exhibit a distinct maximum as a function of the defect concentration. The existence of optimal defect concentrations is explained by the interplay of the on-site, RKKY, and superexchange contributions to the magnetism.

In recent years europium monoxide, EuO, has received considerable attention as a potential material for spintronics, because of its special electronic and magnetic properties. The compound has a rock salt structure, and it is a ferromagnetic insulator below the Curie temperature of $T_C = 69$ K[1–4]. The divalent Eu ions possess a large magnetic moment of 7 μ_B, originating from the half-filled 4*f* states, which are separated by an energy gap of 1.12 eV from the Eu 5*d* conduction band[5]. EuO is suitable as spin filter due to its spin polarization of almost 100%, as demonstrated both by experiment[4,6–8] and theory[9]. Spin filter tunneling junctions (metal/EuO/metal heterojunctions) based on polycrystalline EuO have been studied in various experiments[10–16]. Integration of EuO on semiconducting GaAs[17], GaN[7], and Si[7,18] has been demonstrated. Particularly, the possibility of growth on graphene[19] and topological insulators[20] is interesting for spintronics devices.

The ferromagnetism of EuO, in general, originates from indirect exchange, J_1, and superexchange, J_2. It is widely accepted that the indirect exchange is governed by the Eu 4*f* and 5*d* orbitals[21,22], whereas the superexchange involves the hybridized Eu 4*f* and O 2*p* orbitals[23], where mediation by 6*s* and 5*d* states appears to be important[24,25]. It has been suggested by Ingle and Elfimov[21] that T_C can be enhanced most effectively by reducing the gap between the Eu 4*f* and 5*d* states, and by minimizing the hybridization between the Eu 4*f* and O 2*p* states. In this context, rare earth doping with La, Lu, and Gd, has been studied experimentally[26–36], by model approaches[1,37–39], and by first-principles calculations[21–23,31,33,40–42]. The effects of rare earth doping, which is efficient only for low dopant concentrations, have been explained by modifications of the on-site and RKKY interactions[22]. On the other hand, enhancement of T_C can also be achieved in O deficient EuO[43–45], and by the application of tensile strain[25]. In fact, epitaxial growth of EuO on appropriate substrates can result in a tetragonal or an orthorhombic structure[36].

Commonly used methods for modeling doping effects on the electronic structure of EuO are the virtual crystal approximation[31,40] and the rigid band approximation[33]. First-principles calculations for Gd-doped EuO by the supercell approach (partial substitution of Eu by Gd) have been reported in Ref. 41 without addressing the exchange interaction. Insight into the magnetism has been accomplished in Refs. 22 and 42 for a restricted set of configurations.

In contrast, the purpose of our work is to investigate the effect of Gd doping and O deficiency in the entire concentration range relevant for experiment, focusing on the electronic structure, exchange interaction, and T_C. We will first analyze the effect of Gd doping and afterwards that of O deficiency.

Results

In our first-principles calculations we use a linear combination of atomic orbitals and Troullier-Martins norm-conserving relativistic pseudopotentials (as implemented in the SIESTA code)[46]. The wave functions are expanded in a ζ+polarization basis, except for the Eu 4*f* states for which we use a single-ζ basis. A cutoff of 600 Ry is employed together with $4 \times 4 \times 4$ and $6 \times 6 \times 4$ uniform meshes, respectively, for sampling the Brillouin zones of the cubic and tetragonal phases. To achieve an accurate description of the EuO band gap, we use the local density approximation with on-site Coulomb repulsions (U), and exchange parameters (J)[47,48]. Note that these parameters refer to the microscopic interacting-electron problem; in particular, these J should not be

confused with the exchange interactions of the effective Heisenberg model, to be discussed in connection with Eqs. (1)–(3).

For the Eu 4*f* states we set $J_f = 0.77$ eV[21], but we vary U_f between 8 and 9 eV since the band structure depends critically on the on-site potential of the Eu 4*f* states. A value of $U_f = 8.8$ eV gives the best agreement with the experimental situation (band gap of 1.1 eV, and band splitting of 0.6 eV)[4,6]. Following Ref. 21 we use $J_p = 1.2$ eV and $U_p = 4.6$ eV for the O 2*p* orbitals. Moreover, for the Gd 4*f* orbitals we set $J_f = 0.7$ eV and $U_f = 6.7$ eV[49,50].

The experimental lattice constant of 5.144 Å is used for the rock-salt structure (cubic phase), with four Eu and four O atoms per unit cell. For the tetragonal phase we start from the lattice parameters $a =$ 3.65 Å (inter-planar spacing) and $c = 5.12$ Å (out-of-plane spacing). For both phases, $2 \times 2 \times 2$ supercells are built, which are shown in Fig. 1. These supercells are fully relaxed by means of the conjugate gradient method until the atomic forces have declined below 0.01 eV/Å. We obtain for the cubic phase $a = 5.097$ Å and for the tetragonal phase $a = 3.635$ Å and $c = 5.080$ Å. These values are kept fixed when building the respective structures under Gd doping and O deficiency. Under this constraint, we have carefully relaxed all atomic positions which, of course, is mandatory in order to be able to obtain reliable results. Gd concentrations between 6.25% and 25% are considered, by substituting Eu atoms by Gd; O vacancy concentrations in the same range are achieved by removing O atoms from the supercell. In both cases we distribute the impurities homogeneously in the supercell.

The nearest neighbor (NN, J_1) and next-nearest neighbor (NNN, J_2) exchange interactions for the cubic phase are determined by fixing three spin configurations, and calculating their respective energies: the ferromagnetic one (FM), an antiferromagnetic (AFM) one with the spin direction alternating in the (001) direction (AFM1), and an AFM one with the spin direction changing every second layer in the (001) direction (AFM2). The total energies (per cation) are related to the J_1 and J_2 as follows[51]:

$$\begin{aligned} E_{\mathrm{FM}} &= E_0 + S(S+1)(-12J_1 - 6J_2), \\ E_{\mathrm{AFM1}} &= E_0 + S(S+1)(4J_1 - 6J_2), \\ E_{\mathrm{AFM2}} &= E_0 + S(S+1)(-4J_1 - 2J_2) \end{aligned} \tag{1}$$

where $S = 7/2$. Given J_1 and J_2, an effective Heisenberg model can be defined; and similarly for the tetragonal case (next paragraph).

For the tetragonal phase ($c > a$), we have in-plane NN ($J_{1\|}$), out-of-plane NN ($J_{1\perp}$), in-plane NNN ($J_{2\|}$), and out-of-plane NNN ($J_{2\perp}$) interactions. Note that the term in-plane refers to the *xy*-plane of the tetragonal supercell, which is rotated by 45° with respect to the cubic supercell. To determine the exchange interactions in this case, we have to study five spin configurations: FM, AFM1, AFM2, AFM with the spin direction alternating in the (110) direction (AFM3), and AFM with the spin direction alternating every 2nd layer in the (100) direction (AFM4). The total energies (per cation) are given by:

$$\begin{aligned} E_{\mathrm{FM}} &= E_0 + S(S+1)\left(-4J_{1\|} - 8J_{1\perp} - 4J_{2\|} - 2J_{2\perp}\right), \\ E_{\mathrm{AFM1}} &= E_0 + S(S+1)\left(-4J_{1\|} + 8J_{1\perp} - 4J_{2\|} - 2J_{2\perp}\right), \\ E_{\mathrm{AFM2}} &= E_0 + S(S+1)\left(-4J_{1\|} - 4J_{2\|} + 2J_{2\perp}\right), \\ E_{\mathrm{AFM3}} &= E_0 + S(S+1)\left(4J_{1\|} - 4J_{2\|} - 2J_{2\perp}\right), \\ E_{\mathrm{AFM4}} &= E_0 + S(S+1)\left(4J_{2\|} - 2J_{2\perp}\right). \end{aligned} \tag{2}$$

In mean-field approximation this results in[21]

$$\begin{aligned} T_C^{\mathrm{cubic}} &= \frac{2}{3} S(S+1)(12J_1 + 6J_2), \\ T_C^{\mathrm{tetra}} &= \frac{2}{3} S(S+1)\left(4J_{1\|} + 8J_{1\perp} + 4J_{2\|} + 2J_{2\perp}\right). \end{aligned} \tag{3}$$

We note that the magnetic moments are very localized in all our systems, since they are mainly carried by *f* orbitals, and thus hardly depend on the spin configuration. For example, we obtain for the pristine compound in the cubic phase values of 7.09 μ_B (FM), 7.03 μ_B (AFM1), and 7.05 μ_B (AFM2), and in the tetragonal phase values of 7.09 μ_B (FM), 7.03 μ_B (AFM1), 7.00 μ_B (AFM2), 6.98 μ_B (AFM3), and 7.03 μ_B (AFM4).

In order to clarify the effect of Gd doping for both the cubic and tetragonal phases we determine the density of states (DOS) projected on the Eu 4*f*, 5*d*, Gd 4*f*, 5*d*, and O 2*p* orbitals, see Fig. 2. The dependences of the different exchange terms and of T_C on the dopant concentration are addressed in Fig. 3. We first discuss the results for the pristine structures (0% doping), which are very similar for the cubic and tetragonal phases. For the majority spin channel we distinguish three regions: the conduction band (dominated by Eu 5*d* states), upper valence band (dominated by localized Eu 4*f* states, with some hybridization with O 2*p* and Eu 5*d*), and lower valence band (dominated by O 2*p* states, with significant hybridization with Eu 4*f* and 5*d*). The spin minority channel shows a similar structure but without the Eu 4*f* contributions.

For the cubic phase, exchange interactions of $J_1 = 0.63$ K and $J_2 =$ 0.13 K have been derived from single-crystal inelastic neutron scattering[52], which by Eq. (3) corresponds to $T_C = 88$ K, while we find J_1 = 0.50 K and $J_2 = 0.26$ K and hence a T_C of 80 K, consistent with the experimental result. Note that our effective J ($=J_1 + J_2 = 0.76$ K) agrees with the experimental value. For the tetragonal phase, we obtain $J_{1\|} = 0.54$ K, $J_{2\|} = 0.19$ K, $J_{1\perp} = 0.49$ K, and $J_{2\perp} =$ 0.27 K, from which a mean-field T_C of 77 K is calculated. However, recent experiments on films of cubic and tetragonal EuO with 10 Å thickness have found critical temperatures of 56 K and 53 K, respectively[36]. While the absolute values deviate from our theoretical findings, we note that the difference between the two T_C values is exactly the same (3 K). This is a strong indication for the reliability of our calculations, as far as difference quantities and dependencies (like T_C vs. concentration) are concerned.

The effects of Gd doping on the DOS are similar for the cubic and tetragonal phases, see Fig. 2. The exchange splitting of the Eu 5*d* states at the conduction band edge essentially remains the same as in the pristine system. For increasing Gd doping, the Gd 5*d* and Eu 5*d* majority spin states shift to lower energy, increasing the system's metallicity. Since there are many more Gd 5*d* than Eu 5*d* conduction states occupied, mainly the Gd 5*d* states determine J_1 (combination of on-site and RKKY exchange). The hybridization between the Eu 4*f* and O 2*p* states decreases for increasing Gd doping, which reduces the value of J_2 (superexchange).

For 6.25% Gd doping the stronger exchange interaction between the Gd/Eu 5*d* and Eu 4*f* states (the reduced energy gap supports the *f*-*d* hopping) in combination with the RKKY exchange mediated by the conduction states[22] enhances T_C to around 120 K, both in the cubic

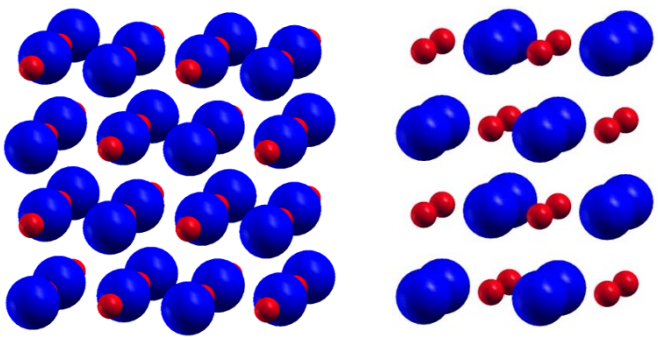

Figure 1 | Structure of EuO in the cubic phase (left) and the tetragonal phase (right). Large spheres (blue) represent Eu, small spheres (red) represent O. The front side is the *xz*-plane.

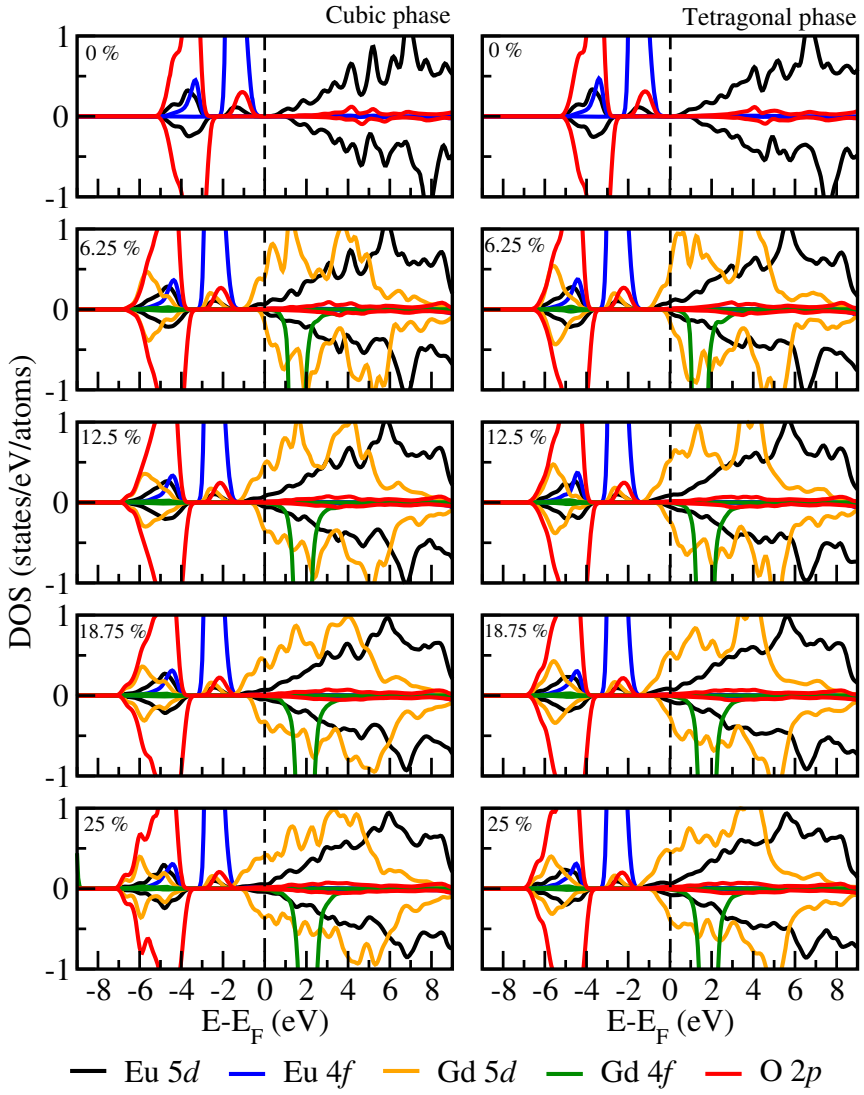

Figure 2 | DOS projected on the Eu 4*f*, 5*d*, Gd 4*f*, 5*d*, and O 2*p* orbitals for the cubic (left) and tetragonal (right) phases of EuO for different Gd concentrations.

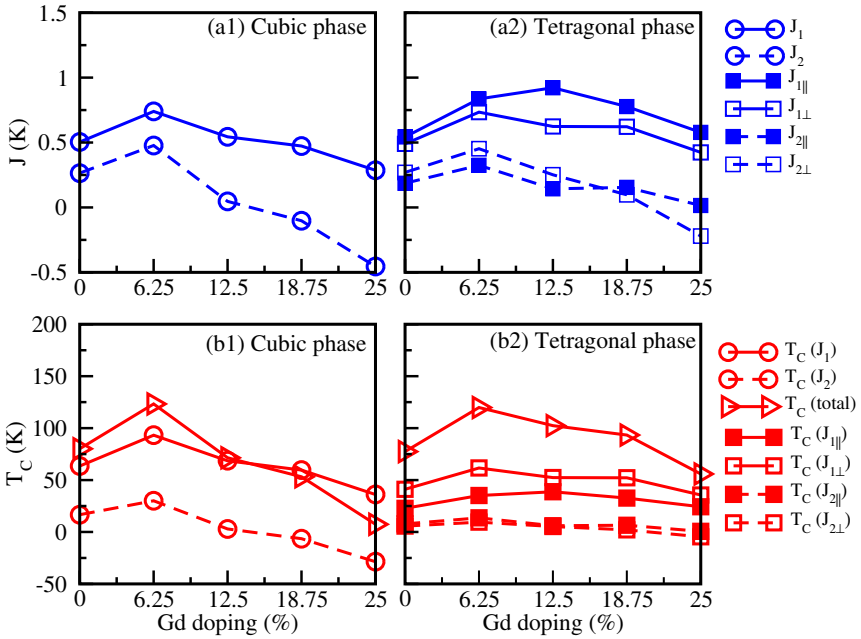

Figure 3 | Exchange interaction and corresponding T_C as a function of the Gd concentration for the cubic phase ((a1), (b1)), and the tetragonal phase ((a2), (b2)).

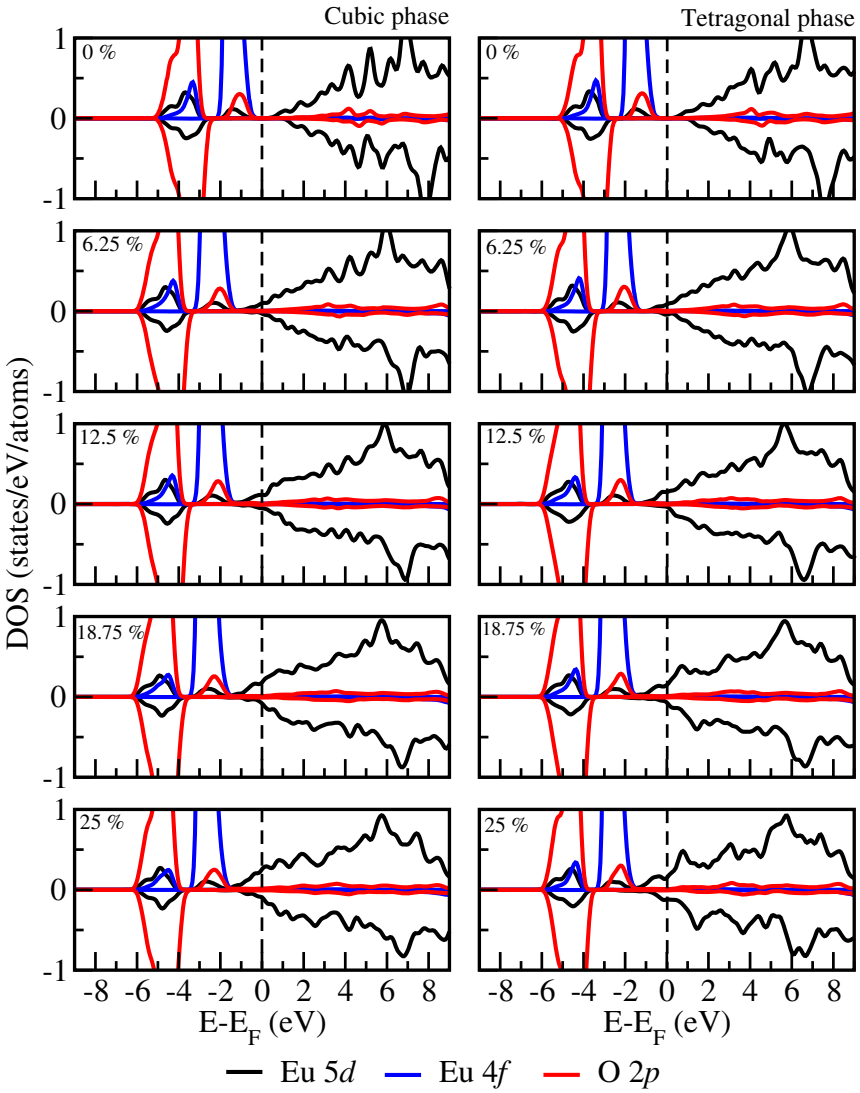

Figure 4 | DOS projected on the Eu 4*f*, Eu 5*d*, and O 2*p* orbitals for the cubic (left) and tetragonal (right) phases of EuO for different O vacancy concentrations.

and tetragonal phases, see Fig. 3(b1),(b2), in good agreement with the experimental value of 129 K for 10% Gd doping[28]. In Ref. 22 a maximal T_C of 160 K for 10% Gd doping has been obtained on the basis of the virtual crystal approximation (using the parameters J_f = 0.6 eV and U_f = 6.1 eV for the Eu 4*f* states). While the validity of the virtual crystal approximation is difficult to assess in this context, we note that T_C depends strongly on the parameter U_f, which in our work was chosen to be U_f = 8.8 eV, in order to reproduce the experimental band gap. With increasing U_f, the band gap opens, hence T_C decreases, and vice versa. On the other hand, Ref. 22 demonstrates that the thermodynamic properties of Gd doped EuO are well captured by the mean field approach.

Above 6.25% Gd doping we observe that the Gd/Eu 5*d* majority spin states shift further towards the Eu 4*f* states, which should enhance T_C. However, the minority spin states start getting filled and, as a consequence, the spin polarization at the Fermi energy is reduced. This compromises the RKKY interaction and therefore effectively lowers J_1 and T_C. In addition, an antiferromagnetic J_2 is observed for 18.75% and higher doping in both phases, which can be explained by enhanced hybridization between the Gd 5*d*, Eu 5*d*, and O 2*p* states: see, for example, the developing joint DOS peaks close to −5 eV.

We next analyze the effects of O deficiency by means of the DOS projected on the Eu 4*f*, 5*d* and O 2*p* orbitals, see Fig. 4, for different O vacancy concentrations. In addition, Fig. 5 addresses the dependences of the different exchange terms and of T_C on the O vacancy concentration. As expected, O deficiency in EuO causes almost rigid shifts of all states to lower energy, giving rise to the well known metal-insulator transition. With increasing O deficiency more and more of the charge donated by the O vacancies occupies the Eu 5*d* conduction bands. It is generally accepted that positive effects on T_C due to O deficiency originate from this extra charge populating the conduction band, and giving rise to enhanced RKKY exchange[1,25,43,44], which corresponds to an increase in J_1. However, also the gap between the majority spin Eu 5*d* and 4*f* states decreases substantially, and the *f*-*d* hopping is enhanced correspondingly, see Fig. 5(a1). The band structure (not shown) demonstrates that the exchange splitting of the Eu 5*d* states at the conduction band edge is reduced significantly for 6.25% O vacancy concentration, as compared to the pristine case, and further slightly decreases for higher O vacancy concentrations.

In addition, the DOS demonstrates that hybridization between the Eu 4*f*, 5*d* and O 2*p* states plays a significant role for the T_C value. We first focus on the cubic phase, see the left hand side of Fig. 4. Hybridization between the Eu 4*f* and O 2*p* states decreases as the O vacancy concentration increases, which enhances J_2, up to 12.5% O vacancy concentration. Afterwards J_2 declines rapidly. According to Fig. 5(b1), T_C increases, as J_1 increases, up to a maximum value of

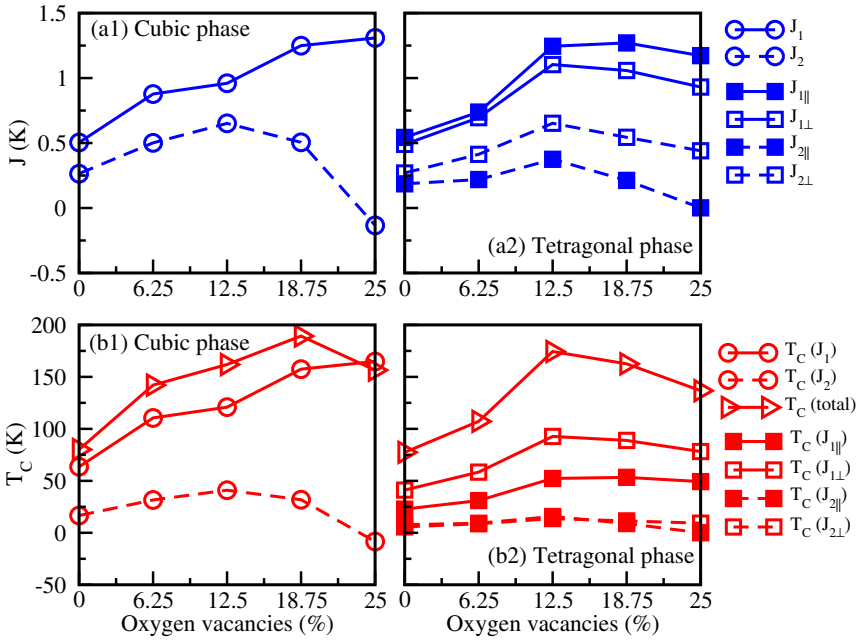

Figure 5 | Exchange interaction and corresponding T_C as a function of the O vacancy concentration for the cubic phase ((a1), (b1)) and the tetragonal phase ((a2), (b2)).

190 K for 18.75% O vacancy concentration, and decreases thereafter, as J_2 decreases. The tetragonal phase, see the right hand side of Fig. 4, overall shows similar characteristics, i.e., $J_{1||}$, $J_{1\perp}$, $J_{2||}$, and $J_{2\perp}$, see Fig. 5(a2), first increase with O deficiency. However, now the Eu 5*d* minority spin states get filled for 12.5% and higher O vacancy concentrations, and J_1 is reduced accordingly, resulting in a maximum in T_C of about 175 K, see Fig. 5(b2).

Discussion

We have performed first principles calculations for both Gd doped and O deficient EuO to clarify the mechanisms that determine the critical temperatures of the cubic and tetragonal phases. We extend previous theoretical considerations for the cubic phase to high defect concentrations, and present the first comprehensive account of the role of defects in the tetragonal phase. The calculated maximum in T_C, as a function of Gd concentration, is in good agreement with the experimental value. The observed behavior is explained by a complex combination of different exchange mechanisms. While both the on-site and RKKY interactions increase with increasing (but low) doping, filling of the Gd 5*d* minority spin states at high doping counteracts the RKKY exchange. In addition, the superexchange is modified at high doping due to growing hybridization between the Gd 4*f* and O 2*p* states. The dependence of T_C on the O deficiency is controlled by a similar mechanism, though now the Eu 5*d* states take over the role of the Gd 5*d* states. As a consequence, optimal values exist both for the Gd dopant and O vacancy concentrations.

1. Mauger, A. & Godart, C. The magnetic, optical, and transport properties of representatives of a class of magnetic semiconductors: The europium chalcogenides. *Phys. Rep.* **141**, 51–176 (1986).
2. Eyert, V. & Nolting, W. Influence of valence instabilities on the Curie-temperature of ferromagnetic 4f-systems. *Solid State Commun.* **60**, 905–911 (1986).
3. Eyert, V. & Nolting, W. Magnetic-nonmagnetic transitions in intermediate-valence systems. *Z. Phys. B* **64**, 341–351 (1986).
4. Steeneken, P. G. *et al.* Exchange Splitting and Charge Carrier Spin Polarization in EuO. *Phys. Rev. Lett.* **88**, 047201 (2002).
5. Dimmock, J. O. Optical Properties of the Europium Chalcogenides. *IBM J. Res. Dev.* **14**, 301–308 (1970).
6. Moodera, J. S., Santos, T. S. & Nagahama, T. The phenomena of spin-filter tunnelling. *J. Phys.: Condens. Matter* **19**, 165202 (2007).
7. Schmehl, A. *et al.* Epitaxial integration of the highly spin-polarized ferromagnetic semiconductor EuO with silicon and GaN. *Nature Mater.* **6**, 882–887 (2007).
8. Melville, A. *et al.* Lutetium-doped EuO films grown by molecular-beam epitaxy. *Appl. Phys. Lett.* **100**, 222101 (2012).
9. Jutong, N. *et al.* Electronic transport through EuO spin-filter tunnel junctions. *Phys. Rev. B* **86**, 205310 (2012).
10. Moodera, J. S. & Santos, T. S. Observation of spin filtering with a ferromagnetic EuO tunnel barrier. *Phys. Rev. B* **69**, 241203(R) (2004).
11. Negusse, E. *et al.* Magnetic characterization of ultrathin EuO films with XMCD. *J. Appl. Phys.* **99**, 08E507 (2006).
12. Santos, T. S. *et al.* Determining Exchange Splitting in a Magnetic Semiconductor by Spin-Filter Tunneling. *Phys. Rev. Lett.* **101**, 147201 (2008).
13. Watson, S. M., Santos, T. S., Borchers, J. A. & Moodera, J. S. Relationship between tunnel magnetoresistance and magnetic layer structure in EuO-based tunnel junctions investigated using polarized neutron reectivity. *J. Appl. Phys.* **103**, 07A719 (2008).
14. Negusse, E. *et al.* Magnetic characterization of ultrathin EuO films with XMCD. *J. Appl. Phys.* **105**, 07C930 (2009).
15. Müller, M., Miao, G. X. & Moodera, J. S. Thickness dependence of ferromagnetic- and metal-insulator transition in thin EuO films. *J. Appl. Phys.* **105**, 07C917 (2009).
16. Müller, M., Miao, G. X. & Moodera, J. S. Exchange splitting and bias-dependent transport in EuO spin filter tunnel barriers. *EPL* **88**, 47006 (2009).
17. Swartz, A. G. *et al.* Epitaxial EuO thin films on GaAs. *Appl. Phys. Lett.* **97**, 112509 (2010).
18. Caspers, C. *et al.* Chemical stability of the magnetic oxide EuO directly on silicon observed by hard x-ray photoemission spectroscopy. *Phys. Rev. B* **84**, 205217 (2011).
19. Swartz, A. G., Odenthal, P. M., Hao, Y., Ruoff, R. S. & Kawakami, R. K. Integration of the Ferromagnetic Insulator EuO onto Graphene. *ACS Nano* **6**, 10063–10069 (2012).
20. Wei, P. *et al.* Exchange-Coupling-Induced Symmetry Breaking in Topological Insulators. *Phys. Rev. Lett.* **110**, 186807 (2013).
21. Ingle, N. J. C. & Elfimov, I. S. Influence of epitaxial strain on the ferromagnetic semiconductor EuO: First-principles calculations. *Phys. Rev. B* **77**, 121202(R) (2008).
22. An, J. M. & Belashchenko, K. D. Electronic structure and magnetic properties of Gd-doped and Eu-rich EuO. *Phys. Rev. B* **88**, 054421 (2013).
23. Wan, X., Dong, J. & Savrasov, S. Y. Mechanism of magnetic exchange interactions in europium monochalcogenides. *Phys. Rev. B* **83**, 205201 (2011).
24. Miyazaki, H. *et al.* Direct Observation of Momentum-Dependent Exchange Interaction in a Heisenberg Ferromagnet. *Phys. Rev. Lett.* **102**, 227203 (2009).
25. Liu, P. *et al.* Sign of the superexchange coupling between next-nearest neighbors in EuO. *Phys. Rev. B* **86**, 224408 (2012).
26. Sutarto, R. *et al.* Epitaxy, stoichiometry and magnetic properties of Gd-doped EuO films on YSZ (001). *Phys. Rev. B* **80**, 085308 (2009).

27. Wang, X. *et al.* Effects of Gd Doping and Oxygen Vacancies on the Properties of EuO Films Prepared via Pulsed Laser Deposition. *IEEE Trans. Magn.* **46**, 1879–1882 (2010).
28. Mairoser, T. *et al.* Is There an Intrinsic Limit to the Charge-Carrier-Induced Increase of the Curie Temperature of EuO? *Phys. Rev. Lett.* **105**, 257206 (2010).
29. Mairoser, T. *et al.* Influence of the substrate temperature on the Curie temperature and charge carrier density of epitaxial Gd-doped EuO films. *Appl. Phys. Lett.* **98**, 102110 (2011).
30. Melville, A. *et al.* Lutetium-doped EuO films grown by molecular-beam epitaxy. *Appl. Phys. Lett.* **100**, 222101 (2012).
31. Santana, J. A. C. *et al.* Effect of gadolinium doping on the electronic band structure of europium oxide. *Phys. Rev. B* **85**, 014406 (2012).
32. Santana, J. A. C. *et al.* The local metallicity of gadolinium doped compound semiconductors. *J. Phys.: Condens. Matter* **24**, 445801 (2012).
33. Shai, D. E. *et al.* Temperature Dependence of the Electronic Structure and Fermi-Surface Reconstruction of $Eu_{1-x}Gd_xO$ through the Ferromagnetic Metal-Insulator Transition. *Phys. Rev. Lett.* **108**, 267003 (2012).
34. Altendorf, S. G. *et al.* Spectroscopic observation of strain-assisted TC enhancement in EuO upon Gd doping. *Phys. Rev. B* **85**, 081201 (2012).
35. Mairoser, T., Loder, F., Melville, A., Schlom, D. G. & Schmehl, A. Influence of chemical doping on the magnetic properties of EuO. *Phys. Rev. B* **87**, 014416 (2013).
36. Melville, A. *et al.* Effect of film thickness and biaxial strain on the curie temperature of EuO. *Appl. Phys. Lett.* **102**, 062404 (2013).
37. Arnold, M. & Kroha, J. Simultaneous Ferromagnetic Metal-Semiconductor Transition in Electron-Doped EuO. *Phys. Rev. Lett.* **100**, 046404 (2008).
38. Burg, S., Stukalov, V. & Kogan, E. On the theory of indirect exchange in EuO. *Phys. Status Solidi B* **249**, 847–853 (2012).
39. Takahashi, M. Electronic and magnetic properties of Gd-doped EuO. *Phys. Rev. B* **86**, 165208 (2012).
40. Miyazaki, H. *et al.* La-doped EuO: A rare earth ferromagnetic semiconductor with the highest Curie temperature. *Appl. Phys. Lett.* **96**, 232503 (2010).
41. Wang, H., Schuster, C. & Schwingenschlögl, U. First principles description of the insulator-metal transition in europium monoxide. *Chem. Phys. Lett.* **524**, 68–72 (2012).
42. Glasbrenner, J. K. *et al.* First-principles calculations of transport and magnetic properties of rare-earth materials. *Proc. SPIE* **8461**, 84610F (2012).
43. Barbagallo, M. *et al.* Experimental and theoretical analysis of magnetic moment enhancement in oxygen-deficient EuO. *Phys. Rev. B* **81**, 235216 (2010).
44. Barbagallo, M. *et al.* Thickness-dependent magnetic properties of oxygen-deficient EuO. *Phys. Rev. B* **84**, 075219 (2011).
45. Monteiro, P. M. S. *et al.* Spatially Homogeneous Ferromagnetism below the Enhanced Curie Temperature in EuO_{1-x} Thin Films. *Phys. Rev. Lett.* **110**, 217208 (2013).
46. Soler, J. M. *et al.* The SIESTA method for ab initio order-N materials simulation. *J. Phys.: Condens. Matter* **14**, 2745–2779 (2002).
47. Anisimov, V. I., Zaanen, J. & Andersen, O. K. Band theory and Mott insulators: Hubbard U instead of Stoner I. *Phys. Rev. B* **44**, 943–953 (1991).
48. Anisimov, V. I., Solvoyev, I. V., Korotin, M. A., Czyzyk, M. T. & Sawatzky, G. A. Density-functional theory and NiO photoemission spectra. *Phys. Rev. B* **48**, 16929–16934 (1993).
49. Anisimov, V. I., Aryasetiawan, F. & Lichtenstein, A. I. J. First-principles calculations of the electronic structure and spectra of strongly correlated systems: the LDA+U method. *J. Phys.: Condens. Matter* **9**, 767–808 (1997).
50. Wang, H., Chroneos, A., Jiang, C. & Schwingenschlögl, U. Special quasirandom structures for gadolinia-doped ceria and related materials. *Phys. Chem. Chem. Phys.* **14**, 11737–11742 (2012).
51. Larson, P. & Lambrecht, W. R. L. Electronic structure and magnetism of europium chalcogenides in comparison with gadolinium nitride. *J. Phys.: Condens. Matter* **18**, 11333–11345 (2006).
52. Mook, H. A. Temperature Dependence of the Spin Dynamics of EuO. *Phys. Rev. Lett.* **46**, 508–511 (1981).

Acknowledgments

We thank T. Archer, L. Chioncel, and I. Rungger for fruitful discussions. The work in Augsburg was supported by the Deutsche Forschungsgemeinschaft (TRR 80). Computational resources have been provided by LRZ Munich, Germany. Research reported in this publication was supported by the King Abdullah University of Science and Technology (KAUST).

Author contributions

N.J. has performed the calculations. T.M., U.E. and U.S. have interpreted the results.

Additional information

Competing financial interests: The authors declare no competing financial interests.

How to cite this article: Jutong, N., Eckern, U., Mairoser, T. & Schwingenschlögl, U. Effect of Gd doping and O deficiency on the Curie temperature of EuO. *Sci. Rep.* **5**, 8038; DOI:10.1038/srep08038 (2015).